frontiers in Remote Sensing

TYPE Original Research
PUBLISHED 14 April 2026
DOI 10.3389/frsen.2026.1812294

OPEN ACCESS

EDITED BY
Celso H. L. Silva-Junior,
Instituto de Pesquisa Ambiental da Amazonia (IPAM), Brazil

REVIEWED BY
Wenjie Fan,
Peking University, China
Ali Suhardiman,
Mulawarman University, Indonesia

*CORRESPONDENCE
Sisipho Ngebe,
sngebe@sansa.org.za

RECEIVED 16 February 2026
REVISED 13 March 2026
ACCEPTED 17 March 2026
PUBLISHED 14 April 2026

CITATION
Ngebe S, Naidoo L, van Deventer H, Tsele P and Qabaqaba M (2026) Assessment of seasonal variations in teal carbon of the palustrine wetland in the Grassland Biome of South Africa using remote sensing.
Front. Remote Sens. 7:1812294.
doi: 10.3389/frsen.2026.1812294

Assessment of seasonal variations in teal carbon of the palustrine wetland in the Grassland Biome of South Africa using remote sensing

Sisipho Ngebe[1,2]*, Laven Naidoo[2,3], Heidi van Deventer [2,4], Philemon Tsele[2] and Mcebisi Qabaqaba[2]

[1]Earth Observation Directorate, South African National Space Agency, Pretoria, South Africa, [2]Department of Geography, Geoinformatics and Meteorology, University of Pretoria, Pretoria, South Africa, [3]Gauteng City-Region Observatory (GCRO), A Partnership of the University of Johannesburg, The University of the Witwatersrand, Johannesburg, The Gauteng Provincial Government and Organised Local Government in Gauteng (SALGA), Johannesburg, South Africa, [4]Council for Scientific and Industrial Research (CSIR), Pretoria, South Africa

Quantifying carbon stocks from the above-ground biomass (AGB) of wetland vegetation across seasons is crucial for assessing ecosystem resilience to anthropogenic and climate pressures. This study aimed to assess differences between summer and winter in aboveground carbon (AGC) of palustrine wetland vegetation using Sentinel-1 and Sentinel-2 data. The Random Forest (RF) and Support Vector Regression (SVR) were implemented with variable importance selection to develop an optimal model from remote sensing derived modelling scenario combinations. Modelling scenarios included field measured Leaf Area index and different combinations of (i) Sentinel-2 derived variables namely vegetation indices (VIs) and reflectance bands, and (ii) Sentinel-1 grey-level co-occurrence matrices, backscatter band ratios, and backscatter channels. Results indicated significant seasonal variation ($p < 0.05$) with higher total teal carbon in summer (155.1 g C/m^2) than winter (115.8 g C/m^2). Large macrophytes particularly Phragmites australis stored the highest carbon (93.04 g C/m^2 in summer; 78.37 g C/m^2 in winter). Sentinel-1-derived models outperformed Sentinel-2-based models for both seasons, achieving R^2 of 0.7–0.8, RMSE of 39.9–69.6 g·m^{-2}, and relative RMSE of 17.3%–21.3%. RF consistently performed better than SVR. Thus, seasonal monitoring of teal carbon provide valuable insights of wetlands vegetation contribution in carbon accounting and sequestration.

KEYWORDS
above-ground biomass, carbon sequestration, essential biodiversity variables, machine learning, Sentinel-1, Sentinel-2

1 Introduction

Inland freshwater wetlands play a critical role in global carbon cycling by storing carbon in vegetation and soils. Carbon stored in these freshwater wetland ecosystems is increasingly referred to as "teal carbon", a concept introduced to distinguish carbon stored in inland wetlands from coastal blue carbon ecosystems such as mangroves, salt marshes, and seagrasses (Nahlik and Fennessy, 2016). Teal carbon ecosystems include shallow inland wetlands such as riverine, lacustrine, and palustrine systems characterised by predominantly freshwater conditions. These ecosystems are important natural carbon sinks and contribute to climate change mitigation through carbon sequestration. Recent studies have applied the

teal carbon framework to evaluate carbon dynamics in inland wetland environments (Kumar and Sharma, 2025) particularly in the assessment of soil organic carbon dynamics. Among the different carbon pools in freshwater wetlands, vegetation biomass represents a key and measurable component for estimating carbon storage and sequestration dynamics. Biomass, particularly above-ground biomass (AGB) of wetland vegetation, is linked to a variety of crucial services such as the provision of nutrients in soils, above ground carbon (AGC) stock quantification, and peat formation. However, wetlands are strongly influenced by seasonality resulting in differences in the carbon and nutrient cycles, water content and energy (Jin et al., 2014; Mitsch et al., 2013). Intensified impacts of anthropogenic and climatic change pressures also exacerbate the decline in freshwater ecosystems, thus affecting the distribution and functioning of these ecosystems (Grundling et al., 2021; Mutanga et al., 2012; Salimi et al., 2021). Monitoring seasonal changes in the AGB is consequently essential for carbon quantification, which plays a pivotal role in quantifying and managing carbon fluxes in grassland ecosystems (Dube et al., 2021). There are still few reliable seasonal estimates of the carbon stock from dry biomass particularly in fresh-water ecosystems of African regions. Current quantification of AGC is largely limited to woody biomass, which does not capture the variability of wetland herbaceous vegetation, particularly in the Grassland Biome which covers only 40% of the extent of the globe (Heidenreich, 2009; Petermann and Buzhdygan, 2021). To understand resilience of palustrine wetlands to anthropogenic and climate variability, timely spatial and temporal monitoring of AGC is therefore critical.

Conventionally, AGB and carbon stock has been quantified through destructive field techniques and allometric equations that relate biomass to key structural attributes particularly in forested environments (Chave et al., 2005; Otukei and Emanuel, 2015). In-field assessments of AGC across wetland vegetation communities showed a higher carbon in the post-summer seasons, compared to the summer and winter seasons, for a palustrine wetland in the temperate regions of India (Lolu et al., 2019). Nonetheless, information gaps persist for palustrine wetlands in semi-arid southern hemisphere regions. Although field methods are crucial for model calibration and validation, they are labour-intensive, time-consuming, and often restricted in remote areas such as in wetlands. Conversely, the advances in remote sensing has increasingly contributed to more accurate and non-destructive estimates of AGB and even in inaccessible locations (Dube et al., 2021; Ramoelo et al., 2015). The estimation of AGB of wetland vegetation using remote sensing is based on correlating biomass with spectral features such as vegetation indices (VIs) and field-collected biophysical parameters (Mutanga et al., 2012; Dube et al., 2021; Ramoelo et al., 2015). These VIs can suppress soil background while significantly improving the sensitivity of the detection of green vegetation when estimating AGB (Mutanga and Skidmore, 2004). Leaf Area Index (LAI) is, for example, a crucial metric for characterising the growth of grassland and wetland vegetation, and it is a strong proxy of the AGB (Van Wijk and Williams, 2005; Naidoo et al., 2019). However, VIs such as the Normalised Difference Vegetation Index (NDVI) reach saturation in areas with high-density biomass (Mutanga and Skidmore, 2004). Alternatively, red edge (RE) region of the electromagnetic spectrum proved to increase the accuracy of AGB estimates over-coming the effect of saturation in areas with dense canopies and moderate to higher AGB (Mutanga and Skidmore, 2004; Ramoelo et al., 2015). Numerous studies have demonstrated the remote sensing data for mapping trends in AGB, revealing significant variations across years, seasons, geographic regions, and in response to various environmental and anthropogenic pressures (Lumbierres et al., 2017; Wang et al., 2022; Li et al., 2021; Ren et al., 2022; Rapiya et al., 2023). While in Southern African region previous studies such as Naidoo et al. (2019) successfully estimated AGB in wetland ecosystems, and Rapiya et al. (2023) focused on seasonal biomass dynamics in rangelands, neither quantified seasonal carbon storage in wetlands. Thus, timely assessments of AGC are still limited.

The accessibility of free Sentinel-1 and Sentinel-2 sensors at a finer spatial resolution of 10 m including the four RE bands offers new opportunities to improve monitoring of wetland vegetation AGB and carbon stock. Optical data also contribute to improved discernment of palustrine wetland vegetation and adjacent terrestrial vegetation, and mapping to different wetland vegetation communities (Van Deventer et al., 2022b). Despite these advantages, several shortcomings are associated with the optical data in estimating vegetation AGB, including the reduced ability to sense the 3D structure of vegetation, signal saturation and cloud obstruction (Guo et al., 2017). Synthetic Aperture Radar (SAR) has become an attractive technology that can be used together with optical data to improve wetland AGB estimates regardless of cloudy condition (Englhart et al., 2011; Sinha et al., 2015). Polarised and co-polarised backscatter channels (VH and VV) have shown to effectively estimate wetland AGB (Naidoo et al., 2019). Even so, radar backscatter signals can be limited in estimating AGB of submerged vegetation in wetlands ecosystems (Gallant, 2015). The analysis of texture measurements is an image processing method that can improve the estimation of AGB by addressing certain existing saturation problems associated with VIs and the C-band wavelength (Kelsey and Neff, 2014). Image texture, such as the grey level co-occurrence matrices (GLCMs) methods, enables provision of structural and geometrical information on vegetation properties (Kelsey and Neff, 2014). Irrespective of tone (i.e., backscatter), texture can enhance spatial information retrieval by raising the saturation level and improving the range of AGB that can be estimated using SAR data. The advancement and integration of machine learning in remote sensing models for estimating AGB in wetlands and grasslands has demonstrated non-linear relationships between remote sensing-derived predictors and field-collected AGB across broader geographical extents (Wan et al., 2018; Naidoo et al., 2019; Li et al., 2021). Machine learning algorithms such as Random Forest (RF), artificial neural networks (ANN) and Support Vector Machines (SVM) improve the robustness and generalization capacity of regression models through modelling which can incorporate many training predictor variables, big data and missing data and can deal with highly collinear variables (Ramoelo et al., 2015). Moreover, these techniques offer variable importance selection which can enhance modelling and reduce model overfitting. Adding to these advancements, the aim of the study was to assess whether the teal carbon derived from AGB of palustrine wetlands differed between the winter and summer seasons in the Grassland Biome of South Africa. The objectives were to: (a) identify the best combination of predictors and optimal

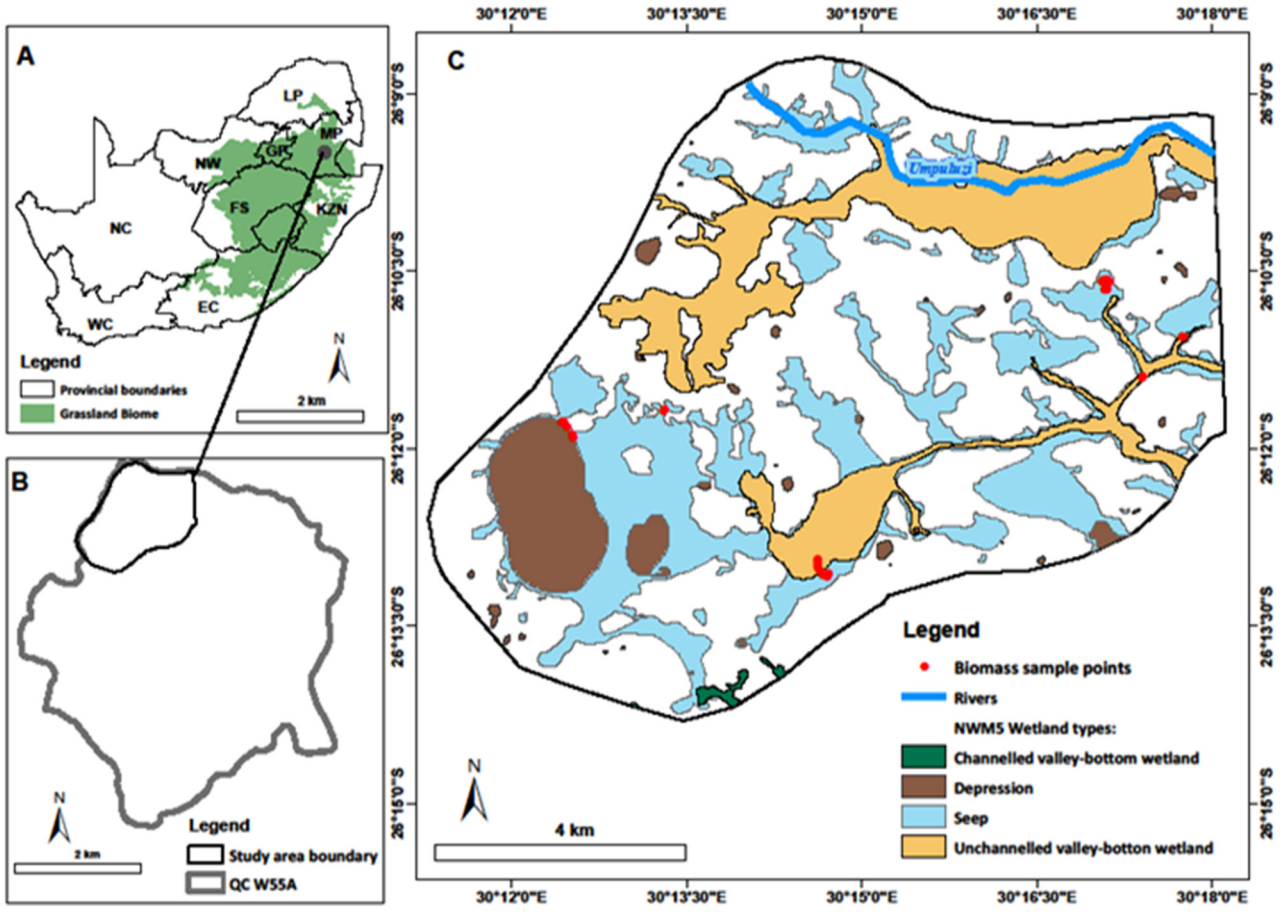

FIGURE 1
Map of the study Area showing **(A)** the extent of the Grassland Biome within South Africa's provinces and the location of the study area in Mpumalanga Province; **(B)** the position of the study area in the northern part of the quaternary catchment (QC) W55A, Within the Mpumalanga Lakes District (MLD); and **(C)** wetland types from the National Wetland Map version 5 (NWM5) with field sampling points in the Tevredenpan study area.

machine learning model for mapping spatial and temporal patterns of AGB in palustrine vegetation; and (d) assess whether teal carbon is different between seasons and across different vegetation communities.

2 Materials and methods

2.1 Study area

The study was conducted in the north-western part of the W55A quaternary catchment, within the Grassland Biome of Mpumalanga Province, South Africa (Figures 1A,B). The catchment is called the Mpumalanga Lakes District (MLD; Figure 1B), where the uprift of the plateau resulted in a large amount (416) of mapped depressions, consisting of both lacustrine and palustrine depressions as well as palustrine seeps and valley-bottom wetlands (Figure 1C) (Sieben et al., 2014; Van Deventer et al., 2020a). Some of the depressions, such as the large Tevredenpan depression (26.2°S; 30.2°E) located in the western part of the study area, combines open water with a large amount of common reed (*Phragmites australis*), which fringe and float on the water (Figure 1C). Nine wetland vegetation communities and one terrestrial vegetation community were previously mapped for wetlands in the MLD (Van Deventer et al., 2020a; Van Deventer et al., 2022b). In general, wetlands in South Africa are considered highly threatened and poorly protected due to factors such invasive species encroachment, agricultural expansion, urbanization, and industrial pollution (Van Deventer et al., 2020a; Fourie et al., 2015).

2.2 Field data collection

Field sampling took place across the summer and winter seasons of 2017 in the study area (Figure 1). The summer visits were made between 27 February 2017 and 2 March 2017 during the peak growth season, and in winter between 27 August 2017 and 1 September 2017 after the peak of winter Van Deventer et al., 2020a). The sample plots in both summer and winter of 6 m × 6 m were selected within homogeneous patches larger than 20 m × 20 m considering Sentinel-1 10 m pixel size. The location of the sample plots was chosen based on homogeneity, of dominant vegetation communities as well as vegetation traits such as the canopy cover, community composition and height. A stratified random sampling method

TABLE 1 Sentinel-1 and Sentinel-2 images acquired in summer and winter for the Tevredenpan study area.

Sensor name	Acquired bands	Acquisition date	Season	Resampled spatial resolution
Sentinel-1A	VH and VV	2017/01/25	Summer	20 m
	VH and VV	2017/08/29	Winter	20 m
Sentinel-2A	13 spectral bands	2017/01/19	Summer	10 m
	13 spectral bands	2017/08/30	Winter	10 m

VH = vertical-horizontal polarization; VV = vertical-vertical polarization.

was implemented for the collection of 32 wet AGB samples for each season where 26 samples were collected in the wetland sections and six samples from the terrestrial section. A Trimble GEO 7X Differential Global Positioning System (Trimble GEO 7X) with a horizontal error of less than <50 cm was used to record the coordinates of the centre point of each plot for the summer season. Subsequently, in the winter sampling campaign, a Garmin 62s GPS was used to locate the centre points of these sampling plots. To cover the representative range of variation in the AGB within each plot, three 0.5 m × 0.5 m quadrants were randomly positioned inside each plot of size 6 m × 6 m and the AGB was physically harvested at the base. Furthermore, at the time of harvesting, the soil was saturated but not fully inundated, thus allowing sampling at the base of the stems. The harvested AGB was later weighed and averaged for the entire plot. In addition, the measured AGB was converted and standardised to g m^{-2}, allowing direct comparison with satellite-derived estimates. The values of dry AGB per plot were then derived by drying the wet AGB for ≥48 h at a temperature of 80 °C using an oven until the weight stabilised using an oven (Naidoo et al., 2019). LAI was included as an additional input variable to improve the estimation of wetland vegetation AGB (Van Wijk and Williams, 2005; Naidoo et al., 2019). Field measurements of LAI were also collected during both summer and winter AGB sampling trips. The LAI Plant canopy Analyser (LiCOR LAI-2200C) was used to obtain observed LAI field values within the three 0.5 m × 0.5 m quadrant sub-plots prior to AGB harvesting. The LAI was computed per quadrant with one reading taken above the canopy and two measurements taken below the vegetation canopy which were then averaged to obtain single LAI value for the entire 6 × 6 m plot. LAI measurements were taken under clear sky conditions, while avoiding obstructions such as shadows that could influence canopy gap detection. The sampling protocol and data utilized in this study was established by Naidoo et al. (2019).

2.3 Remote sensing data acquisition and pre-processing

2.3.1 Sentinel-1 datasets

Sentinel-1A Ground Range Detected (GRD) images, for both winter and summer seasons (Table 1), were downloaded from the Alaska Satellite Facility website (https://search.asf.alaska.edu/#/) considering the field sampling dates in an Interferometric Wide Swath (IW) imaging mode. Images of Sentinel-1A were processed using the Sentinel Application Platform (SNAP) software version 8.0 (Torres et al., 2012; European Space Agency, 2016). The pre-processing of these images included (1) radiometric calibration, (2) multi-looking (3) geometric correction (i.e., terrain correction) and (4) speckle filtering. A Digital Elevation Model (DEM), the Shuttle Radar Topography Mission (SRTM 3 arc second) at 30 m pixel resolution (Farr and Kobrick, 2000), was used for terrain correction to mitigate image distortions caused by topography as well as finding correct geographical coordinates of the image pixels. Multi-looked GRD images for this study had two range looks, two azimuths, the resultant mean ground range pixel or spatial resolution was 20 m and Refined Lee filter was used to further remove or minimise SAR speckle.

2.3.2 Sentinel-2 datasets

The Sentinel-2A MSI is an optical sensor that collects reflectance data from 13 spectral bands and provides two product types: Level-1C (top of atmosphere reflectance) and Level-2A (bottom of atmosphere reflectance). The summer (wet) and winter (dry) Sentinel-2A images were obtained from the US Geological Survey website (https://earthexplorer.usgs.gov/) as Level-1C considering field collection dates (Table 1). The selected Sentinel-2 images were pre-processed in SNAP software, involving (1) atmospheric correction, (2) resampling of the images to 10 m spatial resolution and (3) spatial and spectral bands subsetting. Sentinel-2A (Level 1C) images were converted from top of the atmosphere to Bottom of Atmosphere using the Sen2cor plugin. The configuration of the Sen2cor parameters was based on the values proposed in the user manual (Mueller-Wilm, 2017). The study selected 10 (bands 1, 9 and 10 omitted) of the 13 spectral bands of Sentinel-2A MSI and resampled to 10 m to enhance the characterisation of AGB of wetland vegetation.

2.4 Computation of Sentinel-1A and 2A modelling variables and estimation of LAI

2.4.1 Sentinel-1A predictor variables

The study assessed the potential and efficiency of Sentinel-1A GRD for AGB estimation of wetland vegetation in the Grassland Biome, using GLCM textural metrics, SAR band ratio and backscatters values (Table 2). The GLCM measurement technique has strong adaptability, robustness and it is widely known for its reliability in characterising spatial patterns (Haralick et al., 1973). In this study, eight GLCM textural metrics for both the polarizations bands (VH and VV) were calculated on a single processing window size (9 X

TABLE 2 Summary and formulas of predictor variables from seasonal Sentinel-1A and Sentinel-2A imagery used for above ground biomass modelling.

Sensor	Remote sensing predictor variables		Variable formula/Name	Bands used	References
Sentinel-1A	GLCM texture variables		MEA, VAR, COR, ENT, HOM, CON, SAM, DIS	VH, VV	Haralick et al. (1973)
	Backscatter channels		VH, VV	VH, VV	
	SAR band ratio			VH/VV	
Sentinel-2A	RE VIs	NDVIre5	NIR-RE/NIR + RE	Band 8-Band 5/Band 8+band 5	Gitelson et al. (1996)
		NDVIre6	NIR-RE/NIR + RE	Band 8-Band 6/Band 8+Band 6	
		NDVIre7	NIR-RE/NIR + RE	Band 8-Band 7/Band 8+Band 7	
		SRre5	NIR/RE	Band 8/band 5	
	Traditional VIs	GRVI	GREEN-RED/GREEN + RED	Band 3-Band 4/Band 3+Band 4	Tucker (1979)
		NDVI	NIR-RED/NIR + RED	Band 8-Band 4/Band 8+Band 4	Tucker (1979)
		GNDVI	NIR-GREEN/NIR + GREEN	Band 8-Band 3/Band 8+Band 3	Gitelson et al. (1996)
		SR	NIR/RED	Band 8/Band 4	
	Reflectance bands			B2, B3, B4, B5, B6, B7, B8, B8A, B11, B12	

GNDVI: green normalized difference vegetation index; GRVI: green red vegetation index; NDVI: normalized difference vegetation index; NDVIre5: Normalized Difference Vegetation Index Red-edge 1; NDVIre6: Normalized Difference Vegetation Index Red-edge 2; NDVIre7: Normalized Difference Vegetation Index Red-edge 3; SR: simple ratio; SRre5: Simple Ratio Red-edge 1; and B: bands.

9 pixels) and the following textures were derived: dissimilarity (DIS), mean (MEA), homogeneity (HOM), variance (VAR), entropy (ENT), second angular moment (SAM), contrast (CON), and correlation (COR) (Haralick et al., 1973). The backscatter channels and the polarisation ratio (VH/VV0 was also used as a variable for modelling AGB (Naidoo et al., 2019). The influence of factors such as vegetation structure, moisture levels, canopy roughness, and volumetric scattering in the C-band VV and VH backscatter channels allow them to be useful for assessing wetland biomass. Therefore, Sentenel-1A derived predictor variables for this study included backscatter channels, 16 GLCMs for each VH and VV backscatter channel, and VH/VV band ratio making a total of 19 input variables per season including the field measured LAI.

2.4.2 Sentinel-2A predictor variables

The response of optical data signals in wetland ecosystems is often influenced by the presence of open or standing water which affect the absorption of incoming radiation (Naidoo et al., 2019). Various spectral wavelength regions, however, are known to provide information to assess vegetation conditions in these environments. For instance, the green, NIR and RE regions have proved to be effective and important in assessing wetland vegetation in submerged and non-submerged wetland vegetation. By combining these spectral regions into VIs and band ratios, it enhances the assessment of wetland vegetation parameters. Thus, in this study, eight VIs, which were known to correlate well with AGB estimation, were calculated from the reflectance bands of Sentinel-2A (Li et al., 2021 Naidoo et al., 2019; Mutanga et al., 2012). Four were traditional VIs and the other four were RE-based VIs. The traditional VIs were de-rived from three bands (B3, B4, B8) and the RE VIs from the NIR band (B8) and three RE bands (B5, B6, B7) of Sentinel-2A. Sentinel-2 MSI predictor variables for wetland vegetation AGB estimation in both summer and winter included ten reflectance bands and eight VIs (Table 2) totaling up to 18 per season including field-measured LAI.

TABLE 3 Modelling scenarios used for Leaf Area Index estimation.

Scenarios	Input variables
Scenario 1	Spectral bands (10)
Scenario 2	VIs (8)
Scenario 3	Spectral bands (10) + VIs (8)

VIs = vegetation indices.

2.5 Computation of LAI

Stepwise Multiple Linear Regression (SMLR) (Karatzoglou et al., 2006) was used to find the optimal model for predicting the LAI for the summer and winter season regionally within the study area for AGB mapping in the subsequent steps. Modelling scenarios (Table 3) which included the selected ten spectral bands, and eight VIs of Sentinel-2 were implemented for the estimation of the LAI in RStudio (version 4.0.3). The Akaike Information Criterion (AIC) through the 'stepAIC' function implemented in the 'MASS' package (Ripley et al., 2013) was used for variable selection and the model with lower AIC value was selected for modelling of the LAI. The models were evaluated based on k-10-fold cross-validation. A model with the lowest relative root-mean-square error (relRMSE) was selected for predicting the LAI. The predictors selected in the SMLR model optimal model were stacked as raster layers in R using modelMap package to generate seasonal LAI raster layers for the study area.

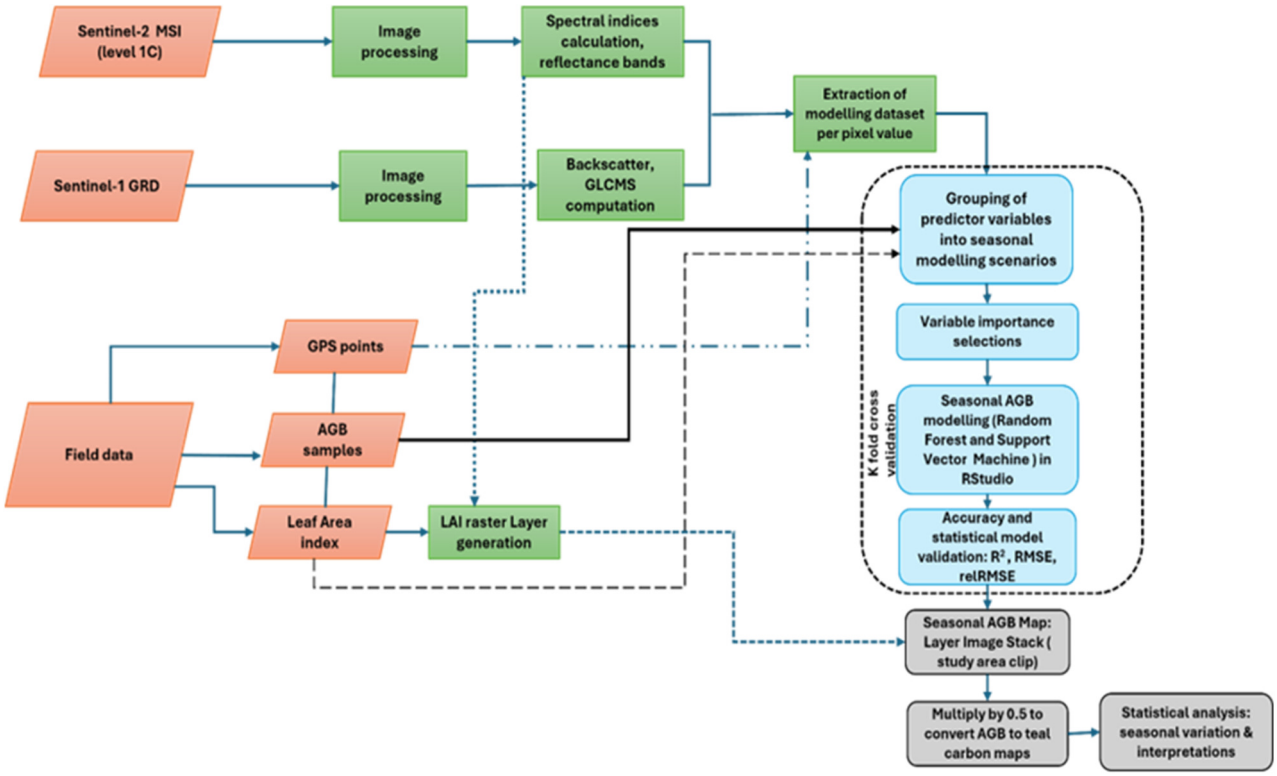

FIGURE 2
Flowchart describing data integration and modelling process of AGC.

TABLE 4 Modelling scenarios implemented in Random Forest and Support Vector Regression for estimation of summer and winter above ground biomass, and numbers in brackets indicating the number of predictor variables.

Scenarios	Sentinel-1A	Sentinel-2A
Scenario 1	GLCMs only (16) + LAI	Reflectance bands (10) +LAI
Scenario 2	Band Ratio (1) + Backscatter (2)	Traditional VIs (4) +LAI
Scenario 3	Backscatter (2) + GLCMs only (16)	RE VIs (4) +LAI
Scenario 4	Backscatter (2) + band ratio (1)	Reflectance bands (10) + RE indices (4) + Traditional VIs (4) +LAI

GLCM = grey-level co-occurrence matrix; LAI = Leaf Area Index; RE = Red-edge band.

2.6 Extraction of seasonal modelling dataset and grouping into modelling scenarios

For extraction of modelling datasets, the raster layers of all the computed input variables from both Sentinel-1A and Sentinel-2A were imported into ArcMap version 10.4.1 (Environmental Systems Research Institute, 2016) to conduct value extraction. The shapefile of the GPS coordinate points representing the centre of each sample plots for each season were used to obtain corresponding pixel value of the Sentinel-1A predictors (backscatter; GLCMs; band ratio) and Sentinel-2A (reflectance; VIs) using the "Extract Multi-values to Points" tool. Thus, this ensured that the extracted pixel values were representative of the sampled locations. The pixel values obtained were then saved to an Excel file, creating the dataset for modelling the AGB in RStudio. The methodology followed to estimate teal carbon from AGB is presented in Figure 2.

2.7 Machine learning algorithms for modelling AGB of palustrine wetland vegetation

The RF and the Support Vector Regression (SVR)S algorithms were implemented as regression models in this study to model AGB of palustrine wetland vegetation. Both models were implemented in RStudio (v4.0.3), with RF using the "randomForest" package (Liaw, 2006) and SVM using the "e1071" package (Karatzoglou et al., 2006). Both models were implemented in different modelling scenarios (Table 4), and a variable important selection method was applied in scenarios with more than ten input variables to enhance the accuracy of the models.

The RF algorithm (Breiman, 2001) is a robust ensemble learning method that improves regression and classification by integrating multiple decision trees. It has been applied in AGB modelling by

analysing the relationships between remote sensing variables and *in situ* biophysical parameters (Mutanga et al., 2012; Naidoo et al., 2019; Li et al., 2021). To select the most important variables in RF models, Variable Selection Using Random Forest (VSURF) function was applied (Genuer et al., 2015). VSURF follows a three-step variable selection procedure, where variables are first ranked based on their importance scores, irrelevant variables are removed through thresholding, and the most informative subset of variables is then selected to optimize model performance (Genuer et al., 2015). A repeated 10-fold cross-validation resampling method (repeated twice) was used to improve model robustness by splitting the data into several equal-sized folds (Richter et al., 2012). Two key RF parameters were optimized: ntree, the number of trees in the model, which was set to 500 as commonly used in literature, and mtry, the number of variables used for node splitting, which ranged between 2 and 12 depending on the number of input parameters used for each modelling scenario.

SVR, the regression implementation of the SVM algorithm (Cortes and Vapnik, 1995) transforms non-linear regression problems into a linear form using kernel functions and is known for its efficiency in handling complex data structures. The Radial Basis Function (RBF) kernel was selected due to its computational efficiency (Wan et al., 2018). For SVR models, the recursive feature elimination (RFE) (Chen and Jeong, 2007) was used for variable importance selection to improve model performance. RFE follows a backward selection process, ranking input variables based on relevance and iteratively removing less significant features based on RMSE (Chen and Jeong, 2007; Guyon et al., 2002). A grid search function was applied to optimize key hyperparameters such as cost and sigma, where multiple candidate values of the cost parameter were automatically evaluated and the value producing the lowest RMSE was selected, while sigma remained at its default value.

Separate RF and SVR models were developed for each season to capture seasonal variations in AGB estimation, ensuring that the best-performing model was selected for each period based on accuracy metrics. Three statistical metrics were used to evaluate the performance of the RF and SVR models: coefficient of determination (R^2), RMSE, and relRMSE (Richter et al., 2012). These measures are widely applied in vegetation biophysical parameter estimation (Naidoo et al., 2019; Li et al., 2021; Tsele et al., 2023). Accuracy assessment was conducted for both RF and SVM seasonal models in R, and the optimal model was selected based on the lowest relRMSE as this metric normalizes RMSE relative to the mean of the observed values, allowing for more reliable comparison between modelling scenarios.

2.8 Spatial mapping of AGB and quantification of teal carbon from AGB

To map the AGB in the study, the predictor variables (used in the optimal modelling scenario), including the LAI raster layer, which was identified as an important variable across all modelling scenarios, were stacked for the spatial mapping process of summer and winter seasonal AGB. The trained optimal models were applied to the raster stack to generate spatial predictions of AGB across the study area for both seasons. To ensure accurate spatial representation, the predictor variables were overlaid and clipped to the study area extent using a study area subset boundary. The mapping procedure was implemented in R statistical software using the 'modelMap,' raster,' and 'rgdal' packages (Bivand et al., 2015; Hijmans et al., 2015; Freeman et al., 2018). The AGB seasonal maps were subsequently converted to seasonal carbon maps. To estimate carbon stocks from AGB a conversion approach indicating that carbon concentrations constitute 50% of the AGB on average was applied (Chave et al., 2005; Houghton et al., 2009). Although the carbon content of wetland herbaceous vegetation may vary slightly among species, typically ranging between 46% and 52%, the use of a 0.50 conversion factor is widely accepted as a default approximation in biomass carbon accounting, and the resulting uncertainty remains within an acceptable range for regional carbon stock assessments. The conversion has also been applied in wetland carbon assessments to estimate carbon stocks from biomass in tropical freshwater wetlands (Dayathilake et al., 2020). Thus, a conversion scaling factor (SF) of 0.50 was applied to the modelled maps of AGB for the summer and winter seasons using Equation 1 to convert them to carbon stock maps. The conversion of the AGB maps was done in ArcMap.

$$C = AGB \times SF \quad (1)$$

Where: C = carbon stock in g C/m2, AGB = above ground biomass (g/m2), and SF = 0.50.

2.9 Assessment of seasonal variation differences in teal carbon storage

To assess seasonal variations in the amount of carbon stored within the AGB in the Tevredenpan study area, 176 random sampling points were generated within wetland and terrestrial areas defined by the National Wetland Map version 5 (NWM5) boundary polygons (Van Deventer et al., 2020b) using the "Random Points Inside Polygons" tool in QGIS (v3.18). Points outside the NWM5 polygons were considered terrestrial, while those within or inside the polygons were considered wetlands. For both the summer and winter seasons, carbon values were extracted from the seasonal maps using the created random points. To quantify the seasonal variations several measures of variability including standard deviation (SD), coefficient of variation (COV%) and the mean were computed. An independent unpaired T-test was also performed at a 95% confidence interval to assess the statistical significance.

The study further determined seasonal variations in carbon storage across nine wetland vegetation communities between the summer and winter season. The vegetation types analysed include Three-awned grass (*Aristida spp.*), nepalese reed grass (Arundinella *nepalensis*), Sedges (*Carex spp.*), grass-sedge, Love Grass (*Eragrostis plana*), soft rush (*Juncus effuses*), *Phragmites australis*, Sedge dominant, red grass (*Themeda triandra*), and Wet-grass, using the delineated existing vegetation boundary polygons from Van Deventer et al. (2022b). Each vegetation community polygon was selected using the "Select by Attribute" function in QGIS based on the vegetation class name and exported as individual polygon layers. The QGIS Random Points Inside Layer Bounds tool was then used to generate 80 random points within each vegetation community polygon and were used to extract carbon per vegetation type from the predicted seasonal carbon maps. The two-way ANOVA was implemented to assess the statistical differences across the nine

10.3389/frsen.2026.1812294

TABLE 5 Sentinel-1A and Sentinel-2A based assessment of significant variable selection in RF and SVR models with over ten input predictors for summer and winter seasons.

Sentinel-1	SS1		WS1	
	RF VSURF	SVR RFE	RF VSURF	SVR RFE
Scenario 1: GLCMs (16) +LAI	LAI, vhMEAN	LAI, vhMEAN, vhVariance	vhVariance, LAI	LAI, vhMEAN, vhVariance, vvMEAN, vvVariance
Scenario 3: Backscatter (2) + GLCMs only (16) +LAI	LAI, vhMEAN, VH	LAI, vhMEAN, vhVariance	VH, LAI, vhVariance	VH, LAI, vhVariance, vhMEAN, VV
Scenario 4: Backscatter (2) + Band ratio (1) + GLCMs (16) +LAI	LAI, vhMEAN, vhVariance, VH	LAI, vhVariance, vhMEAN, VH, vvCorrelat	VH, LAI, vhVariance	VH, LAI, vhVariance, vhMEAN, VV
Sentinel-2	**SS2**		**WS2**	
	RF VSURF	SVR RFE	RF VSUR	SVR RFE
Scenario 1: Reflectance bands (10) +LAI	LAI, B4, B3, B6, B8	LAI, B4, B5, B3, B7	LAI, B12	LAI, B12
Scenario 4: Reflectance bands (10) + RE indices (4) + Traditional VIs (4) +LAI	LAI, SR, NDVI, B4, B3, GNDVI, B5	LAI, SR, B8, NDVI, B5, B4	LAI, NDVI SRre5, NDVIre5, B12	LAI, SR, B12, SRre5, NDVI, NDVIre5

SS1 = Summer Sentinel-1; WS1 = Winter Sentine-1. SS2 = Summer Sentinel-2; WS2 = Winter Sentine-2.

vegetation communities. The relationship between season and vegetation type as well as their interaction were then tested at a confidence interval of 95%. ANOVA is a statistical method that is important to determine variations between the means of various variables. Furthermore, a post-hoc Tukey's HSD grouping with letters was implemented to identify the specific vegetation groups that showed notable seasonal variations in the amount of carbon stored in the AGB for both the summer and winter seasons.

3 Results

3.1 Variable importance selection

According to the results of variable importance selection in Tables 5 selected important predictors varied in both the RF and SVR models across the investigated seasons. Sentinel-1 results illustrated that the LAI was a prominent predictor in both RF and SVR models (Table 5), indicating its importance in AGB estimation in both summer and winter. VH backscatter and textures (vhMEAN and vhVariance) also influenced AGB estimation in the study area for in both seasons. Furthermore, the ratio between VH and VV was not selected as an important predictor in the estimation of AGB for both seasons when looking at the trend of the input variables in Scenario 4 (backscatter, band ratio, GLCMs, and LAI). When examining the selected variables in Sentinel-2 models, the LAI was selected as the most important variable among other variables for Scenario 1 and Scenario 4 modelling. In summer variable important selection in RF and SVR also showed that the red-edge (RE), green (B3), red (B4), B5, and B6 bands as important predictors, respectively. Conversely, the selection of important predictors in winter revealed that SWIR band (B12) was the only important reflectance band, among others. Modelling Scenario 4 showed that NDVI and Simple Ratio (SR) were important selected traditional indices when all variables were included in RF and SVR for both seasons. In addition, the red-edge derived indices such as NDVIre5 and SRre5 were most important predictors of wetland AGB.

3.2 Accuracy of modelling scenarios and comparison between RF and SVR algorithms in predicting wetland AGB for the summer and winter season

The results of RF and SVR model accuracies in Table 6 revealed that RF predicted AGB better with Sentinel-1 variables (GLCM textures, backscatter, and LAI) compared with Sentinel-2 variables in summer season using Scenario 3. However, Scenario 1 revealed that RF attained higher accuracy with GLCM textures and LAI accounting for relRMSE = 20.9%, R^2 = 0.785, and RMSE = 67.582 g·m^{-2} in winter season. The optimal model for Sentinel-2 derived variables which include combined spectral bands and vegetation indices achieved highest accuracy at Scenario 4 with RF (R^2 = 0.753, RMSE = 49.269 g·m^{-2}, and relRMSE = 20.0%) for summer. RF accuracy values increased to R^2 = 0.768, RMSE = 65.699 g·m^{-2}, and relRMSE = 38.4% for winter AGB estimation. Meanwhile, Sentine-2 models achieved higher R^2 values. It is worth noting that these Sentinel-2 models had big error margins in comparison to Sentinel-1, especially in winter season. For all modelling Scenarios RF outperformed SVR attaining lower RMSE and relRMSE values. The AGB maps were produced using RF Scenario 3 (SAR GLCM textures, C-band backscatter, and LAI) and RF Scenario 1 (SAR GLCM textures and LAI) for summer and winter, respectively.

The scatterplots in Figure 3 depict the comparison between observed and predicted AGB for the study area. The findings showed the RF models to be closer to the 1:1 line compared to the SVR models. Even though SVR models illustrated significant correlation during winter (Figure 3D), especially in Scenario 3 for Sentinel-1

TABLE 6 Random Forest and Support Vector Regression remote sensing validation model accuracies of Sentinel-1 and Sentinel-2 derived modelling scenarios for estimation of wetland above-ground biomass with 10-fold cross-validation across summer and winter.

	Summer						Winter					
	RF			SVR			RF			SVR		
Sentinel-1	R^2	RMSE	relRMSE	R^2	RMSE	relRMSE	R^2	RMSE	relRMSE	R^2	RMSE	relRMSE
Scenario 1	0.709	40.919	17.538	0.723	46.861	38.328	0.785	67.582	**20.885**	0.795	64.209	35.206
Scenario 2	0.699	44.005	17.546	0.716	44.794	36.568	0.736	72.944	21.53	0.763	64.953	39.682
Scenario 3	0.735	39.848	**17.286**	0.708	44.188	36.753	0.805	67.063	21.371	0.852	59.887	**33.287**
Scenario 4	0.697	44.278	17.796	0.726	44.294	36.719	0.777	68.778	21.774	0.773	65.442	37.773
Sentinel-2	R^2	RMSE	relRMSE	R^2	RMSE	relRMSE	R^2	RMSE	relRMSE	R^2	RMSE	relRMSE
Scenario 1	0.644	52.856	**19.61**	0.651	51.071	**37.891**	0.651	51.071	**37.891**	0.644	73.267	40.726
Scenario 2	0.665	52.865	22.051	0.643	48.890	38.674	0.643	48.890	38.674	0.691	68.911	46.198
Scenario 3	0.629	50.352	21.918	0.702	52.937	41.983	0.702	52.937	41.983	0.640	69.775	43.839
Scenario 4	0.753	49.269	20.009	0.652	50.595	40.374	0.652	50.595	40.374	0.768	65.699	**38.447**

Bold values indicate selected model results.
relRMSE = relative root mean square error; R^2 = coefficient of determination; RMSE = root mean square error.

(R^2 = 0.852), the high relRMSE values indicated a greater degree of variability in prediction errors.

3.3 Spatial patterns in carbon of wetland vegetation

Spatial mapping of above ground carbon within the study area is shown in Figure 4. The results illustrated varying carbon stock patterns, with noticeable lower carbon in winter (Figure 4A) and high carbon in summer (Figure 4B). Along seasonal seep wet-lands (D-2), there is moderate carbon values in summer (160–180 g C/m^2), but low coverage is observed in winter <160 g C/m^2 in winter (E-2), likely due to reduced vegetation productivity. The distribution of carbon in the Tevredenpan depression (D-1 & E-1) as well as the valley-bottom wetlands (D-3 & E-3) characterized by the presence of *Phragmites australis* and Bulrush (*Typha capensis*) presented high carbon stock in both seasons (205–280 g C/m^2). Additionally, the Agricultural fields (D-4) also showed high carbon stock coverage (190–220 g C/m^2) in summer than in winter (E-4).

3.4 Seasonal variations in estimated carbon stocks

3.4.1 Differences in carbon storage between wetland and terrestrial across summer and winter season

According to Table 7 the total mean carbon storage in summer was higher (155.1 g C/m^2) compared to winter (115.8 g C/m^2), indicating a 39.2 g C/m^2 seasonal decrease in carbon accumulation. The mean teal carbon storage in wetlands declined from 78.3 g C/m^2 (summer) to 58.6 g C/m^2 (winter), a 25% reduction indication of high carbon content in summer than the winter season. Terrestrial HGM type also illustrated high mean values of the terrestrial carbon in summer 76.8 g C/m^2 compared to 57.3 g C/m^2 in winter. The comparison of mean carbon values of terrestrial and wetland carbon showed no significant difference (<2% difference and p-value >0.05) although terrestrial carbon was slightly higher than wetland carbon in summer. A similar pattern was observed in winter, where the mean carbon values for terrestrial and wetland carbon also showed no significant difference (<1% difference, $p > 0.05$). The winter season showed greater relative variability in winter compared to summer.). Overall, the comparison of the mean values in groups (summer–winter) demonstrated a statistically significant seasonal difference ($p < 0.05$) in estimated carbon.

Tukey HSD groupings and the seasonal carbon stock (g C/m^2 ± SD) of wetland vegetation communities in the study area are summarized in Table 8 and Figure 5. Phragmites australis (grouped a) had the largest carbon stock in both summer and winter, with values of 93.04 ± 20.34 g C/m^2 and 78.37 ± 25.99 g C/m^2, respectively. In contrast, the lowest carbon stocks were observed in Eragrostis spp. and Themeda spp. (66.16 ± 13.89 g C/m^2 in summer; 53.26 ± 15.56 g C/m^2 in winter) and Sedge dominant communities (67.51 ± 13.17 g C/m^2 in summer; 53.15 ± 16.29 g C/m^2 in winter), grouped in e and d, respectively. The distinction between high and low carbon storing values of vegetation communities are indicated by clear statistical variations using Tukey groupings. The Carex spp. and Juncus effusus vegetation types were not significant, both grouped in b. Surprisingly, Aristida spp, Eragrostis spp and Themeda spp revealed extreme observations (Figure 5). In addition, all other vegetation communities without shared letters are significantly different at the 95% confidence level.

4 Discussions

Biomass, particularly AGB of wetland vegetation, is linked to a variety of crucial services such as the provision of nutrients in soils, above-ground carbon (AGC) stock quantification, and peat

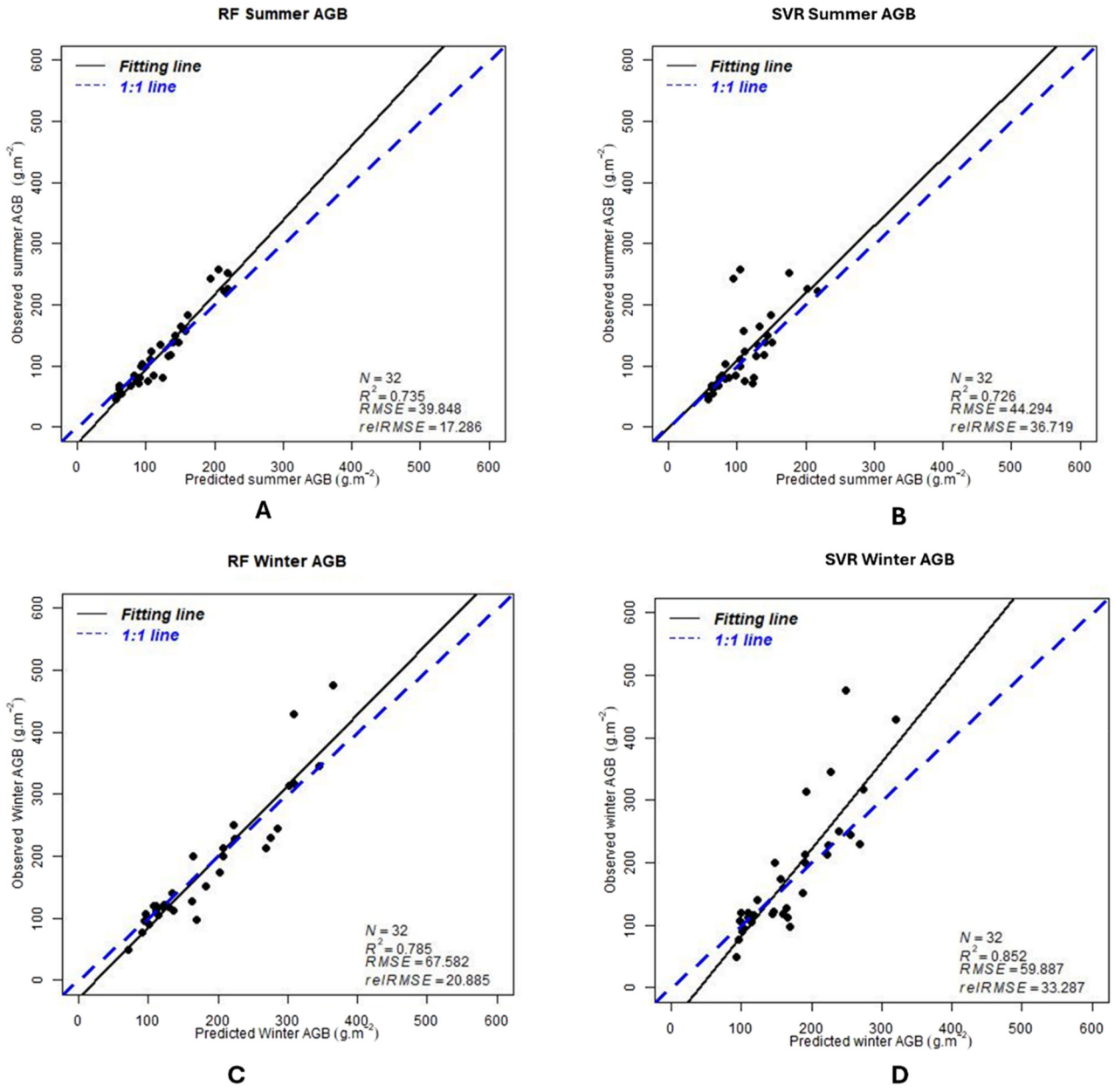

FIGURE 3
Seasonal accuracies of observed versus predicted AGB density scatterplots across seasons using the RF and SVR models after 10-fold cross validation. **(A)** GLCMs, backscatter; **(B)** SVR summer model; **(C)** RF winter model; **(D)** SVR winter mode and dotted blue line = 1:1 trend line.

formation. Monitoring seasonal changes in the AGB is essential for carbon quantification, which plays a pivotal role in quantifying and managing carbon fluxes in grassland ecosystems. This study assessed use integrated remote sensing variables derived from Sentinel-1A and Sentinel-2A imagery for predicting wetland AGC using machine learning to contribute to carbon accounting initiatives and reliable remote sensing-based models of AGB and carbon stock. Based on the best-performing model, the mapped results indicated that the above-ground carbon (AGC) differed across seasons and vegetation communities in the study area allowing for targeted land management interventions. The details of these findings have been outlined in the following paragraphs below.

4.1 Importance of remote sensing variables and accuracies in sensor modelling scenarios in estimating AGC

The results indicated that Sentinel-1 models performed better than Sentinel-2 models. The combination of Sentinel-1 GLCM textures with backscatter improved the accuracy in summer (R^2 = 0.7, RMSE = 39.9 g·m^{-2}, relRMSE = 17.3%) compared to reflectance bands, VIs, and RE bands (R^2 = 0.8, RMSE = 49.3 g·m^{-2}, relRMSE = 20.0%). SAR-based models also performed better in winter (R^2 = 0.8, RMSE: 67.6–69.7 g·m^{-2}, relRMSE: 20.9%–21.3%). The higher penetration capabilities of SAR irrespective of cloud cover, which enable better extraction of structural plant information

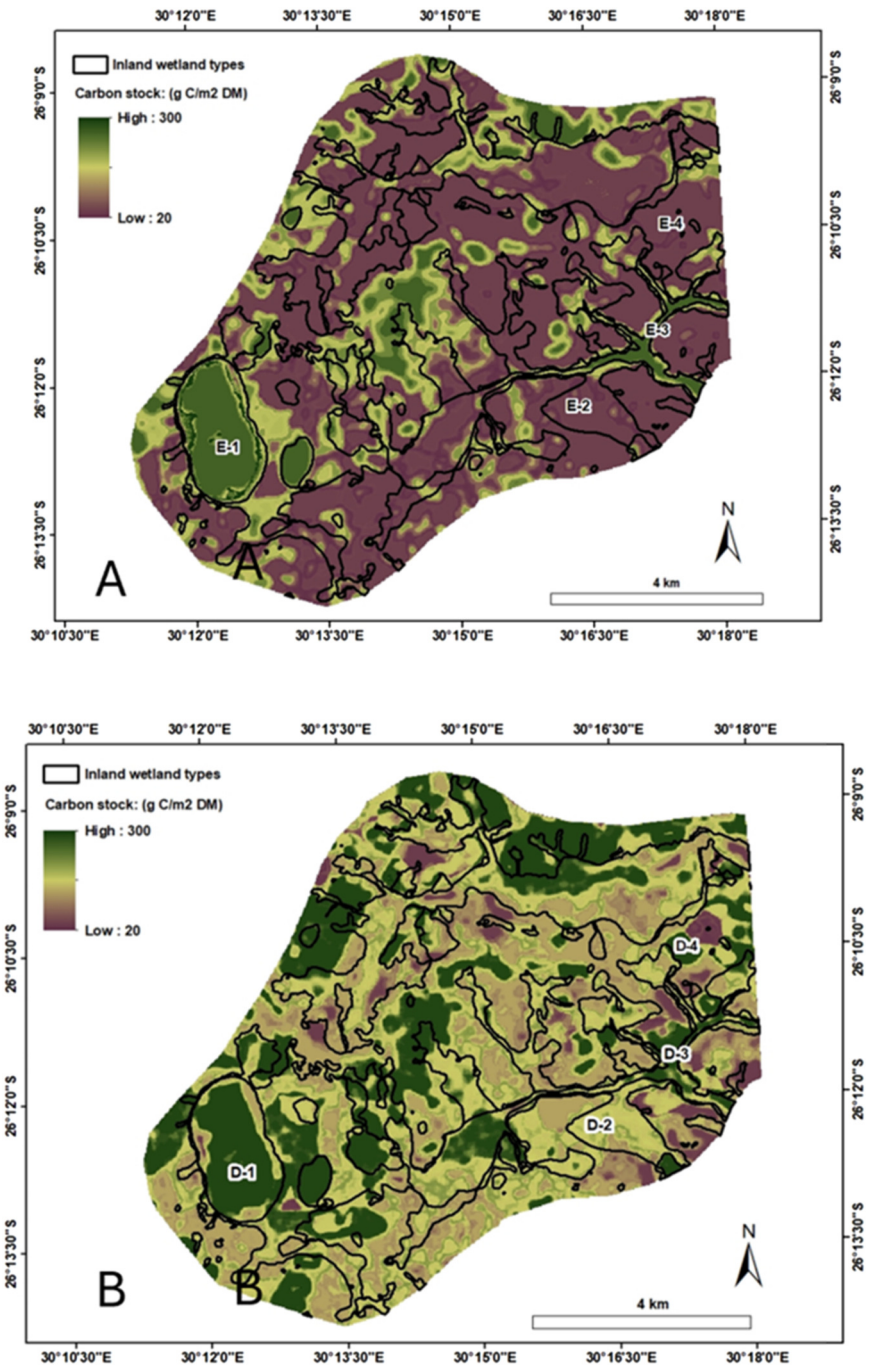

FIGURE 4
Spatial patterns of Above ground carbon stock. **(A)** = winter AGC map; **(B)** = summer AGB map.

in wetlands, such as double bounce scattering between water, emergent, and flooded vegetation, may be attributed to the improved performance of SAR models in this work. Furthermore, the findings indicate that the integration of SAR textures (9 x 9 window size) particularly derived from VH (vhMEAN and VhVariance) and polarimetric features (especially VH) improves the estimation of AGB of wetland vegetation. Textural features play a vital role in estimating vegetation structural parameters, as they capture the spatial arrangement and relationships of pixels within a specified neighbourhood (Kelsey and Neff, 2014). It is worth noting that performance of textural features in modelling AGB may vary depending on spectral characteristics, window size, and vegetation types. The VH backscatter is sensitive to volumetric scattering, especially in vegetation with volumetric structures (such as reeds compared to grasses), whereas VV is often affected by surface roughness (Laurin et al., 2018). Recent studies used textures from optical datasets in wetlands (Li et al., 2021) or were mostly conducted in other environments, such as the forests (Chen et al., 2018; Argamosa et al., 2018) and mangroves (Navarro et al., 2019). This study

TABLE 7 Descriptive statistical table with variations in predicted carbon maps across summer and winter season in Tevredenpan study site.

Season	Realm Carbon type	N	Min	Mean (g C/m^{-2})	Max	SD	COV	p-value <0.05
Summer	Wetland	176	33.5	78.3	109.1	20.1	25.6	No
	Terrestrial	176	31.3	76.8	112.7	21.5	28.0	
	Total	350		155.1				
Winter	Wetland	176	38.630	58.599	98.539	20.672	35.278	No
	Terrestrial	176	39.596	57.250	96.611	18.602	32.494	
	Total	350		115.849				
Summer – Winter				Summer: 77.5 Winter: 58.0				Yes

COV = co-efficient variation, SD = standard deviation, N = total number of random points per season, min = minimum, and max = maximum.

TABLE 8 Seasonal comparison of carbon Stock with Tukey HSD Groups across vegetation types.

Vegetation type	N	Location	Summer mean carbon stock (g C/m^2) ± SD	Turkey HSD grouping	Winter mean carbon stock (g C/m^2) ± SD	Turkey HSD grouping
Arundinella nepalensis	80	Wetland	77.03 ± 17.06	bc	55.96 ± 18.55	d
Aristida spp.	80	Wetland	75.54 ± 14.97	cd	57.84 ± 18.23	cd
Carex spp.	80	Wetland	84.05 ± 16.33	b	72.33 ± 22.86	ab
Eragrostis spp. and *Themeda* spp.	80	Terrestrial	66.16 ± 13.89	e	53.26 ± 15.56	d
Grass-sedge communities	80	Wetland	77.38 ± 16.54	bc	57.35 ± 18.99	cd
Juncus effusus	80	Wetland	84.08 ± 18.68	b	66.59 ± 19.87	bc
Phragmites australis	80	Wetland	93.04 ± 20.34	a	78.37 ± 25.99	a
Sedge dominant	80	Wetland	67.39 ± 18.14	de	53.15 ± 16.29	d
Wet-grass community	80	Wetland	74.26 ± 18.01	cde	58.55 ± 18.93	cd

SD = standard deviation, N = total number of random points for each vegetation type.

therefore extends the existing body of knowledge by using SAR C-band, textural, and polarimetric features with machine learning models to estimate seasonal teal carbon from herbaceous AGB in palustrine wetlands. The study provides an opportunity to test this approach in other environments with greater variability such as lacustrine in the Southern Africa region. Despite Sentinel-1 outperforming Sentinel-2 models, the SWIR band (B12) notably proved to be the most effective for AGB modelling during the dormant season, aligning with findings from (Hemati et al., 2024; Ramoelo and Cho, 2014). Likewise, the LAI was identified to significantly correlate with seasonal AGB in all modelling scenarios for this study. In line with other studies, LAI plays a critical role in estimating AGB (Naidoo et al., 2019; Van Wijk and Williams, 2005). The VIs minimize the influence of soil background and environment noise in remote sensing data overcoming sensor saturation problem (Heidenreich, 2009). This is especially crucial in wetland areas due to the low reflectance associated with wetlands that are either permanently or seasonally saturated. It is important to note that the spatial mismatches between field plot size and satellite resolution may have affected the reliability of extracted pixel values resulting to low or intermediate model accuracy. This challenge is pronounced especially in heterogeneous wetland environments where moisture variability and standing water influence spectral and backscatter signals. Nonetheless, this study demonstrates that both Sentinel-1 and Sentinel-2 datasets can effectively track seasonal carbon changes stored in wetland AGB.

4.2 Comparative performance of machine learning algorithms

Comparative analysis of ML algorithms in estimating seasonal AGB illustrated that the RF model outperformed (relRMSE = 17.3%) the SVR model (relRMSE = 36.7%). RF exhibited strong predictive performance owing to its ability to reduce overfitting, robustness regardless of data distribution (Mutanga et al., 2012). Chen et al. (2018) discovered that SVR outperformed RF and ANN in terms of predictive ability in forest AGB and Adam et al. (2014) observed no significant differences between SVR and RF. Our results are in line with several studies that have shown how accurate RF is in estimating AGB in wetlands and grasslands (Wan et al., 2018; Naidoo et al., 2019; Rapiya et al., 2023). However, these studies did not do seasonal comparative performance of different machine

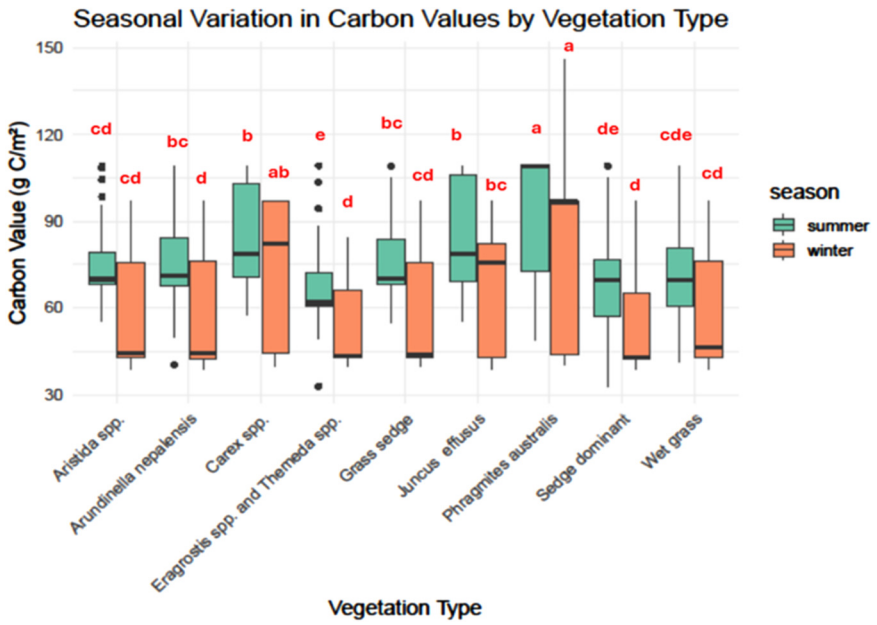

FIGURE 5
Seasonal shifts in AGC of palustrine wetland vegetation communities.

learning models at different seasons (i.e. wet and dry seasons). Thus, the findings in this study further emphasize the importance of machine learning algorithms and their capability to detect non-linear relationships between remote sensing variables and field-measured biophysical parameters at different temporal scales. The reliability of machine learning models used to estimate vegetation biophysical parameters, such as AGB, is influenced by the quality of the calibration and validation datasets, which may contain errors that reduce predictive accuracy. The low accuracy in some of the models in this study can be attributed to the limited number of field samples collected per season which may have affected the accuracy of the predictive models. Small training datasets can reduce the ability of machine learning algorithms to capture the full variability of vegetation structure and environmental conditions across the study area, which may increase model uncertainty and reduce generalization capability. According to Morais et al. (2021) the limited number of field samples used for training and validation may reduce the accuracy of biomass prediction models. The low performance of SVR may also be attributed to poor optimization and tuning of hyperparameter (Cherkassky and Ma, 2004; Wan et al., 2018). Biomass prediction models may also be influenced by underlying environmental factors such as moisture content and seasonal hydrological variability which affect both remote sensing signal and vegetation growth in wetland environments. Incorporating such environmental variables into machine learning frameworks alongside remote sensing data could enhance model performance and robustness across seasons.

4.3 Seasonal variation in the spatial patterns and quantified AGC

The predicted results of the spatial distribution patterns of carbon stocks ranged from 30 g C/m^2 to 300 g C/m^2 across seasons, based on the integrated Sentinel-1 variables in RF model. The seasonal seep wetlands demonstrated moderate ranges of carbon stock (160–180 g C/m^2) in summer, while in winter, lower ranges (<160 g C/m^2) were evident. The study results suggested a statistical seasonal significance ($p < 0.05$) between summer and winter illustrating that the overall total carbon was higher in summer (155.1 g C/m^2) than in winter (115.8 g C/m^2), further emphasising the influence of seasonal dynamics on carbon content stored in the AGB of wetland vegetation. The presence of dominant wetland vegetation communities such as *Phragmites australis* and *Typha capensis* which are less palatable at the study site resulted in high spatial patterns of carbon stock along valley-bottom wetlands and depressions in both summer and winter. Additionally, the inundation and seasonal saturation in some wetland types of limit cattle movement, thereby reducing grazing pressure on these plant species (Naidoo et al., 2019). Although the impacts of winter fires were not clearly visible in our study area, such events frequently alter distribution and reduce AGB, which may contribute to the decrease in the overall carbon stock. Findings by Syman (2004) and Rapiya et al. (2023), have also alluded that in semi-arid and tropical natural rangelands of South Africa, the impact of fires significantly influence the distribution of AGB.

In the moist highland grasslands of Mpumalanga, Little et al. (2015) also showed that intense fires occurring at the peak of the dry season resulted in reduction of vegetation, thereby reducing biomass and the density of plant material. The increased photosynthesis during the wet growing season results in peak biomass and subsequently high accumulation of carbon content in summer (Mitsch et al., 2013; Sinha et al., 2015; Lolu et al., 2019; Salimi et al., 2021). In a temperate wetland with macrophytes in Hokersar, India, for example, Lolu et al. (2019) found above-ground carbon stocks that averaged 244.9 g C/m^2 in the summer and 188.8 g C/m^2 in the winter. However, Lolu et al. (2019) conducted in field

measurements and did not utilize remote sensing data, thus our study further highlights the potential of using both Sentinel-1 and Sentinel-2 derived variables in quantifying teal carbon from AGB in palustrine wetland. The results also showed non-significant difference ($p > 0.05$) in carbon storage between wetland and adjacent terrestrial areas. Although wetlands are typically associated with higher carbon storage, this may be attributed to the dominance of herbaceous vegetation communities across both environments in the study site which may have comparable seasonal productivity and biomass accumulation patterns. In addition, several factors affect wetlands within the South African Grassland Biome, including grazing pressure, fire disturbances, and land-use changes such as urbanization and agriculture. These pressures can influence vegetation productivity across both wetland margins and adjacent terrestrial grasslands and may result in similar levels of AGB storage.

Our study also showed that vegetation communities were statistically significant between seasons with high mean carbon stock values in summer than winter. Large macrophytes such as *Phragmites australis* (range: 90.04–78.37 g C/m^2) predicted higher in both seasons compared to sedge dominant species (range: 67.39–53.15 g C/m^2). Previous literature have also suggested that these macrophytes store significant quantities of biomass and carbon (Mutanga et al., 2012). Factors such geographic setting, land use practices, climate conditions, and vegetation type may influence the primary productivity in wetland vegetation ecosystems. Extreme observations were also noted in some vegetation communities within the study area (*Aristida spp. and Eragrostis spp. and Themeda spp.*; Figure 5). The outliers could be due to site-specific conditions or ecological factors such as species composition, phenology influencing localised carbon accumulation. During different seasons, natural ecosystems can undergo seasonal changes due to their natural cycles and due to anthropogenic pressures, which can also reflect the accumulated carbon at the individual wetland vegetation community level. The outcomes of this work help land managers understand the locality of the bulk of their wetland carbon reserves across the landscape, which continue to grow and store carbon across seasons due to the water discharge dynamics of such wetland systems (i.e. captured in taller, evergreen and sturdier wetland species communities) and also help identify other wetland communities (e.g. dryland grass communities), which are more vulnerable to seasonal shocks. Land use practices which alter the water table, local temperatures and vegetation community composition can drastically affect the wetland carbon store capacity and sustainable practices of wetland conservation are thus encouraged.

5 Conclusion

This study assessed and map seasonal teal carbon differences derived from the AGB of wetland vegetation in the grassland biome of the Mpumalanga Province, South Africa using machine learning algorithms with different variable combinations from Sentinel-1A GRD and Sentinel-2 MSI data. The AGC differed across seasons and vegetation communities in the study area showed higher values of AGC in summer specifically large macrophytes such as Phragmites australis. The predicted carbon maps also illustrated spatial differences in the spatial distribution of teal carbon across both seasons. Incorporating texture measurements derived from Sentinel-1 improved the estimation of teal carbon, with Sentinel-1A performing better than Sentinel-2A. Furthermore, the results revealed that the RF regression machine algorithm performed better compared to the SVR algorithm. This study therefore provides a novel contribution by integrating remote sensing variables for seasonal analysis, carbon quantification, and monitoring carbon dynamics in a wetland ecosystem. Seasonal estimation of teal carbon using remote sensing would enhance how vegetation in wetlands contributes to sequestration of carbon and thus contributes to improved carbon accounting initiatives and long-term monitoring of wetlands.

Data availability statement

The data analyzed in this study is subject to the following licenses/restrictions: Data available upon request. Requests to access these datasets should be directed to sisiphongebe@gmail.com.

Author contributions

SN: Writing – original draft, Methodology, Software, Visualization, Writing – review and editing, Formal Analysis. LN: Conceptualization, Methodology, Writing – review and editing, Data curation, Funding acquisition, Supervision. HvD: Data curation, Conceptualization, Methodology, Supervision, Writing – review and editing, Funding acquisition. PT: Supervision, Writing – review and editing. MQ: Software, Visualization, Formal Analysis, Writing – review and editing.

Funding

The author(s) declared that financial support was received for this work and/or its publication. This research was funded by South African National Space Agency, Water Research Commission (Project No. project K5/2545) and Council for Scientific and Industrial Research.

Conflict of interest

The author(s) declared that this work was conducted in the absence of any commercial or financial relationships that could be construed as a potential conflict of interest.

Generative AI statement

The author(s) declared that generative AI was not used in the creation of this manuscript.

Any alternative text (alt text) provided alongside figures in this article has been generated by Frontiers with the support of artificial intelligence and reasonable efforts have been made to ensure accuracy, including review by the authors wherever possible. If you identify any issues, please contact us.

Publisher's note

References

Adam, E., Mutanga, O., Odindi, J., and Abdel-Rahman, E. M. (2014). Land-Use/Cover classification in a heterogeneous coastal landscape using RapidEye imagery: evaluating the performance of random forest and support vector machines classifiers. *Int. J. Remote Sens.* 35 (10), 3440–3458. doi:10.1080/01431161.2014.903435

Argamosa, R. J. L., Blanco, A. C., Baloloy, A. B., Candido, C. G., Dumalag, J. B. L. C., Dimapilis, L. L. C., et al. (2018). Modelling above ground biomass of mangrove forest using Sentinel-1 imagery. ISPRS annals of photogrammetry. *Remote Sens. & Spatial Inf. Sci.* 4 (3). doi:10.5194/isprs-annals-IV-3-13-2018

Bivand, R., Keitt, T., Rowlingson, B., Pebesma, E., Sumner, M., Hijmans, R., et al. (2015). Package 'rgdal': bindings for the geospatial data abstraction library. Available online at: https://cran.r-project.org/web/packages/rgdal/index.html (Accessed October 15, 2017).

Breiman, L. (2001). Random forests. *Mach. Learn.* 45, 5–32. doi:10.1023/A:1010933404324

Chave, J., Andalo, C., Brown, S., Cairns, M. A., Chambers, J. Q., Eamus, D., et al. (2005). Tree allometry and improved estimation of carbon stocks and balance in tropical forests. *Oecologia* 145 (1), 87–99. doi:10.1007/s00442-005-0100-x

Chen, X. W., and Jeong, J. C. (2007). "Enhanced recursive feature elimination," in *Sixth international conference on machine learning and applications (ICMLA 2007)* (Cincinnati, OH, USA), 429–435. doi:10.1109/ICMLA.2007.35

Chen, L., Ren, C., Zhang, B., Wang, Z., and Xi, Y. (2018). Estimation of forest above-ground biomass by geographically weighted regression and machine learning with sentinel imagery. *Forests* 9 (10), 582. doi:10.3390/f9100582

Cherkassky, V., and Ma, Y. (2004). Practical selection of SVM parameters and noise estimation for SVM regression. *Neural Netw.* 17 (1), 113–126. doi:10.1016/S0893-6080(03)00169-2

Cortes, C., and Vapnik, V. (1995). Support-vector networks. *Mach. Learn.* 20, 273–297. doi:10.1007/BF00994018

Dayathilake, D. D. T. L., Lokupitiya, E., and Wijeratne, V. P. I. S. (2020). Estimation of aboveground and belowground carbon stocks in urban freshwater wetlands of Sri Lanka. *Carbon Balance and Management*, 15 (1), 17. doi:10.1186/s13021-020-00152-5

Dube, T., Shoko, C., and Gara, T. W. (2021). Remote sensing of aboveground grass biomass between protected and non-protected areas in Savannah rangelands. *Afr. J. Ecol.* 59 (3), 687–695. doi:10.1111/aje.12861

Englhart, S., Keuck, V., and Siegert, F. (2011). Aboveground biomass retrieval in tropical forests—The potential of combined X- and L-Band SAR data use. *Remote Sens. Environ.* 115 (5), 1260–1271. doi:10.1016/j.rse.2011.01.008

Environmental Systems Research Institute (Esri) (2016). *ArcGIS for desktop*. Redlands, CA, USA: Environmental Systems Research Institute.

European Space Agency (ESA) (2016). SNAP – ESA sentinel application platform v2.0.2 (S1TBX). Available online at: http://step.esa.int.

Farr, T. G., and Kobrick, M. (2000). Shuttle radar topography mission produces a wealth of data. *Eos, Trans. Am. Geophys. Union* 81, 583–585. doi:10.1029/EO081i048p00583

Fourie, L., Rouget, M., and Lötter, M. (2015). Landscape connectivity of the grassland biome in Mpumalanga, South Africa. *Austral Ecol.* 40 (1), 67–76. doi:10.1111/aec.12169

Freeman, E. A., Frescino, T. S., and Moisen, G. G. (2018). ModelMap: an R package for model creation and map production. *R J.* 4, 6–12.

Gallant, A. L. (2015). The challenges of remote monitoring of wetlands. *Remote Sens.* 7 (8), 10938–10950. doi:10.3390/rs70810938

Genuer, R., Poggi, J. M., and Tuleau-Malot, C. (2015). VSURF: an R package for variable selection using random forests. *R J.* 7 (2), 19–33. doi:10.32614/RJ-2015-018

Gitelson, A. A., Kaufman, Y. J., and Merzlyak, M. N. (1996). Use of a green channel in remote sensing of global vegetation from EOS-MODIS. *Remote Sens. Environ.* 58 (3), 289–298. doi:10.1016/S0034-4257(96)00072-7

Grundling, P.-L., Grundling, A. T., Van Deventer, H., and Le Roux, J. P. (2021). Current state, pressures and protection of South African peatlands. *Mires Peat* 27, 26. doi:10.19189/MaP.2020.OMB.StA.2125

Guo, M., Li, J., Sheng, C., Xu, J., and Wu, L. (2017). A review of wetland remote sensing. *Sensors* 17 (4), 777. doi:10.3390/s17040777

Guyon, I., Weston, J., Barnhill, S., and Vapnik, V. (2002). Gene selection for cancer classification using support vector machines. *Mach. Learn.* 46, 389–422. doi:10.1023/A:1012487302797

Haralick, R. M., Shanmugam, K., and Dinstein, I. H. (1973). Textural features for image classification. *IEEE Trans. Syst. Man, Cybern.* SMC-3 (6), 610–621. doi:10.1109/TSMC.1973.4309314

Heidenreich, B. (2009). *What are the global temperate grasslands worth? A case for their protection: a review of current research on their total economic value. Report prepared for the world temperate grasslands conservation initiative*. Gland, Switzerland: IUCN. Available online at: https://www.iucn.org/content/what-are-global-temperate-grasslands-worth-a-case-their-protection (Accessed February 27, 2024).

Hemati, M., Mahdianpari, M., Shiri, H., and Mohammadimanesh, F. (2024). Integrating SAR and optical data for aboveground biomass estimation of coastal wetlands using machine learning: multi-scale approach. *Remote Sens.* 16 (5), 831. doi:10.3390/rs16050831

Hijmans, R. J., Van Etten, J., Cheng, J., Mattiuzzi, M., Sumner, M., Greenberg, J. A., et al. (2015). Package raster. *R. Package* 734, 473.

Houghton, R. A., Hall, F., and Goetz, S. J. (2009). Importance of biomass in the global carbon cycle. *J. Geophys. Res. Biogeosciences* 114 (G2). doi:10.1029/2009JG000935

Jin, Y., Yang, X., Qiu, J., Li, J., Gao, T., Wu, Q., et al. (2014). Remote sensing-based biomass estimation and its spatio-temporal variations in temperate grassland, Northern China. *Remote Sens.* 6 (2), 1496–1513. doi:10.3390/rs6021496

Karatzoglou, A., Meyer, D., and Hornik, K. (2006). Support vector machines in R. *J. Stat. Softw.* 15, 1–28. doi:10.18637/jss.v015.i09

Kelsey, K. C., and Neff, J. C. (2014). Estimates of aboveground biomass from texture analysis of 684 landsat imagery. *Remote Sens.* 6 (7), 6407–6422. doi:10.3390/rs6076407

Kumar, S., and Sharma, L. K. (2025). Assessing spatial and seasonal variability in soil organic carbon fractions of teal carbon in semi-arid Ramsar wetlands of India as a natural climate solution. *Discov. Soil* 2, 66. doi:10.1007/s44378-025-00085-w

Laurin, G. V., Balling, J., Corona, P., Mattioli, W., Papale, D., Puletti, N., et al. (2018). Above-ground biomass prediction by Sentinel-1 multitemporal data in central Italy with integration of ALOS2 and Sentinel-2 data. *J. Appl. Remote Sens.* 12 (1), 016008. doi:10.1117/1.JRS.12.016008

Li, C., Zhou, L., and Xu, W. (2021). Estimating aboveground biomass using Sentinel-2 MSI data and ensemble algorithms for grassland in the Shengjin Lake wetland, China. *Remote Sens.* 13 (8), 1595. doi:10.3390/rs13081595

Liaw, A. (2006). *Package RandomForest: Breiman and Cutler's random forest for classification and regression*. Available online at: http://cran.r-project.org/web/packages/randomForest/randomForest.pdf.

Lolu, A. J., Ahluwalia, A. S., Sidhu, M. C., and Reshi, Z. A. (2019). Carbon sequestration potential of macrophytes and seasonal carbon input assessment into the Hokersar Wetland, Kashmir. *Wetlands* 39 (3), 453–472. doi:10.1007/s13157-018-1092-8

Lumbierres, M., Méndez, P. F., Bustamante, J., Soriguer, R., and Santamarie, L. (2017). Modeling biomass production in seasonal wetlands using MODIS NDVI land surface phenology. *Remote Sens.* 9 (4), 392. doi:10.3390/rs9040392

Mitsch, W. J., Bernal, B., Nahlik, A. M., Mander, Ü., Zhang, L., Anderson, C. J., et al. (2013). Wetlands, carbon, and climate change. *Landsc. Ecol.* 28 (4), 583–597. doi:10.1007/s10980-012-9758-8

Morais, T. G., Teixeira, R. F., Figueiredo, M., and Domingos, T. (2021). The use of machine learning methods to estimate aboveground biomass of grasslands: a review. *Ecol. Indic.* 130, 108081. doi:10.1016/j.ecolind.2021.108081

Mueller-Wilm, U. (2017). *Sentinel 2 MPC – sen2Cor configuration and user manual*. European Space Agency ESA, 1–56.

Mutanga, O., and Skidmore, A. K. (2004). Narrow band vegetation indices overcome the saturation problem in biomass estimation. *Int. J. Remote Sens.* 25, 3999–4014. doi:10.1080/01431160310001654923

Mutanga, O., Adam, E., and Cho, M. A. (2012). High density biomass estimation for wetland vegetation using WorldView-2 imagery and random forest regression algorithm. *Int. J. Appl. Earth Observation Geoinformation* 18, 399–406. doi:10.1016/j.jag.2012.03.012

Nahlik, A., and Fennessy, M. (2016). Carbon storage in US wetlands. *Nat. Commun.* 7, 13835. doi:10.1038/ncomms13835

Naidoo, L., Van Deventer, H., Ramoelo, A., Mathieu, R., Nondlazi, B., and Gangat, R. (2019). Estimating above ground biomass as an indicator of carbon storage in vegetated wetlands of the grassland biome of South Africa. *Int. J. Appl. Earth Observation Geoinformation* 78, 118–129. doi:10.1016/j.jag.2019.01.021

Navarro, J. A., Algeet, N., Fernández-Landa, A., Esteban, J., Rodríguez-Noriega, P., and Guillén-Climent, M. L. (2019). Integration of UAV, Sentinel-1, and Sentinel-2 data for mangrove plantation aboveground biomass monitoring in Senegal. *Remote Sens.* 11 (1), 77. doi:10.3390/rs11010077

Otukei, J. R., and Emanuel, M. (2015). Estimation and mapping of above ground biomass and carbon of Bwindi impenetrable national park using ALOS PALSAR data. *South Afr. J. Geomatics* 4 (1), 1–13. doi:10.4314/sajg.v4i1

Petermann, J. S., and Buzhdygan, O. Y. (2021). Grassland biodiversity. *Curr. Biol.* 31 (19), R1195–R1201. doi:10.1016/j.cub.2021.06.060

Ramoelo, A., and Cho, M. A. (2014). "Dry season biomass estimation as an indicator of rangeland quantity using multi-scale remote sensing data," in 10th International Conference on African Association of Remote Sensing of Environment (AARSE) 2014 (Johannesburg: University of), 27–31.

Ramoelo, A., Cho, M. A., Mathieu, R., Madonsela, S., van de Kerchove, R., Kaszta, Z., et al. (2015). Monitoring grass nutrients and biomass as indicators of rangeland quality and quantity using random forest modelling and WorldView-2 data. *Int. J. Appl. Earth Observation Geoinformation* 43, 43–54. doi:10.1016/j.jag.2014.12.010

Rapiya, M., Ramoelo, A., and Truter, W. (2023). Seasonal evaluation and mapping of aboveground biomass in natural rangelands using Sentinel-1 and Sentinel-2 data. *Environ. Monit. Assess.* 195, 1544. doi:10.1007/s10661-023-12133-5

Ren, Y., Mao, D., Li, X., Wang, Z., Xi, Y., and Feng, K. (2022). Aboveground biomass of marshes in northeast China: spatial pattern and annual changes responding to climate change. *Front. Ecol. Evol.* 10, 1043811. doi:10.3389/fevo.2022.1043811

Richter, K., Atzberger, C., Hank, T. B., and Mauser, W. (2012). Derivation of biophysical variables from Earth observation data: validation and statistical measures. *J. Appl. Remote Sens.* 6 (1), 063557. doi:10.1117/1.JRS.6.063557

Ripley, B., Venables, B., Bates, D. M., Hornik, K., Gebhardt, A., Firth, D., et al. (2013). Package 'mass. *CRAN R.* 538, 113–120.

Salimi, S., Almuktar, S. A., and Scholz, M. (2021). Impact of climate change on wetland ecosystems: a critical review of experimental wetlands. *J. Environ. Manag.* 286, 112160. doi:10.1016/j.jenvman.2021.112160

Sieben, E. J. J., Mtshali, H., and Janks, M. (2014). National wetland vegetation database: classification and analysis of wetland vegetation types for conservation planning and monitoring. *Water Res. Comm. (WRC).*

Sinha, S., Jeganathan, C., Sharma, L. K., and Nathawat, M. S. (2015). A review of radar remote sensing for biomass estimation. *Int. J. Environ. Sci. Technol.* 12, 1779–1792. doi:10.1007/s13762-015-0750-0

Syman, H. A. (2004). Estimating the short-term impact of fire on rangeland productivity in a semi-arid climate of South Africa. *J. Arid Environments* 59 (4), 685–697. doi:10.1016/j.jaridenv.2004.02.002

Torres, R., Snoeij, P., Geudtner, D., Bibby, D., Davidson, M., Attema, E., et al. (2012). GMES Sentinel-1 mission. *Remote Sens. Environ.* 120, 9–24. doi:10.1016/j.rse.2011.05.028

Tsele, P., Ramoelo, A., and Qabaqaba, M. (2023). Development of the grass LAI and CCC remote sensing-based models and their transferability using Sentinel-2 data in heterogeneous grasslands. *Int. J. Remote Sens.* 44 (8), 2643–2667. doi:10.1080/01431161.2023.2205982

Tucker, C. J. (1979). Red and photographic infrared linear combinations for monitoring vegetation. *Remote Sens. Environ.* 8 (2), 127–150. doi:10.1016/0034-4257(79)90013-0

Van Deventer, H., Naidoo, L., Cho, M. A., Job, N. M., Linström, A., Sieben, E., et al. (2020a). Establishing remote sensing toolkits for monitoring freshwater ecosystems under global change. *Water Res. Comm. Rep. (WRC).*

Van Deventer, H., Van Niekerk, L., Adams, J., Dinala, M. K., Gangat, R., Lamberth, S. J., et al. (2020b). National Wetland Map 5: an improved spatial extent and representation of inland aquatic and estuarine ecosystems in South Africa. *Water SA* 46 (1), 66–79. doi:10.17159/wsa/2020.v46.i1.7887

Van Deventer, H., Linström, A., Naidoo, L., Job, N., Sieben, E. J. J., and Cho, M. A. (2022b). Comparison between Sentinel-2 and WorldView-3 sensors in mapping wetland vegetation communities of the grassland biome of South Africa, for monitoring under climate change. *Remote Sens. Appl. Soc. Environ.* 28, 100875. doi:10.1016/j.rsase.2022.100875

Van Wijk, M. T., and Williams, M. (2005). Optical instruments for measuring leaf area index in low vegetation: application in arctic ecosystems. *Ecol. Appl.* 15 (4), 1462–1470. doi:10.1890/03-5354

Wan, R., Wang, P., Wang, X., Yao, X., and Dai, X. (2018). Modelling wetland aboveground biomass in the Poyang Lake national nature reserve using machine learning algorithms and Landsat-8 imagery. *J. Appl. Remote Sens.* 12 (4), 046029. doi:10.1117/1.JRS.12.046029

Wang, Y., Shen, X., Tong, S., Zhang, M., Jiang, M., and Lu, X. (2022). Aboveground biomass of wetland vegetation under climate change in the Western songnen plain. *Front. Plant Sci.* 13, 941689. doi:10.3389/fpls.2022.941689